# Original polymorphism in a naphthalene bisimide $\pi$-conjugated organogelator: a complex interplay between hydrogen bonding and heterocycle $\pi$-stacking

Morgane Diebold, Elliot Christ, Laure Biniek, Lydia Karmazin, Benoît Heinrich, Christophe Contal, Suhrit Ghosh, Philippe Mesini, Martin Brinkmann

# Original polymorphism in a naphthalene bisimide π-conjugated organogelator : a complex interplay between hydrogen bonding and heterocycle π-stacking

Morgane Diebold,[a] Elliot Christ,[a] Laure Biniek,[a] Lydia Karmazin,[b] Benoît Heinrich,[c] Christophe Contal[a], Suhrit Ghosh[d], Philippe Mesini[a] and Martin Brinkmann[a]

[a] Institut Charles Sadron, CNRS-Université de Strasbourg, 23 rue du Loess, Strasbourg 67034, France

[b] Institut de Chimie de Strasbourg, 1 rue Blaise Pascal, 67008 Strasbourg, France

[c] Institut de Physique et Chimie des Matériaux de Strasbourg (IPCMS), UMR 7504 CNRS-Université de Strasbourg (UdS), 23 rue du Loess, 67037 Strasbourg Cedex 08, France

[d] Indian Association for the Cultivation of Science, Polymer Science Unit, 2A & 2B Raja S. C. Mullick Rd., Kolkata, India.

*Corresp. authors:* *martin.brinkmann@ics-cnrs.unistra.fr*

*Philippe.mesini@ics-cnrs.unistra.fr*

*psusg2@iacs.res.in*

## Abstract

This study focuses on the structure of different supramolecular assemblies formed in the gel phase and in the solid state by a naphthalene-bisimide organogelator: N,N'-di(1-(3,4,5-tri(octyloxy)benzamido))eth-1yl naphthalene-1,4,5,8 tetracarboxylic acid bisimide (NDI2). This molecule is formed by a naphthalene bisimide core with symmetric dendrons composed of a flexible alkyl linker, an amide group and a trialkoxyphenyl group. The structure, especially the original polymorphism of this molecule, was correlated with optical and electronic properties in the solid state. Four polymorphs have been prepared in pure form: a dried gel phase, a quenched metastable liquid crystalline phase, a crystalline phase and its sister phase with molten alkyl side chains. The molecular packing of those phases was determined from X-ray and electron diffraction as well as high resolution TEM. UV-vis and infrared spectroscopy of the polymorphs uncover the nature of intermolecular π-stacking and H-bonding interactions. In the fibrils of the gel phase, NDI2 molecules form columnar stacks with the fiber axis corresponding to the H-bonding direction between amide groups. The crystalline phase shows an unusual packing such that each NDI is π-stacked between two phenyl groups of the adjacent NDI2 molecules. In the metastable LC phase NDI2 molecules assemble into $6_1$ supramolecular helices further grouped in a frustrated trigonal unit cell. Temperature-dependent TEM, UV-vis and FTIR helped unveil the molecular reorganization upon transformation between these different polymorphs. Finally, a global phase diagram has been obtained.

**Figure for Title of content**

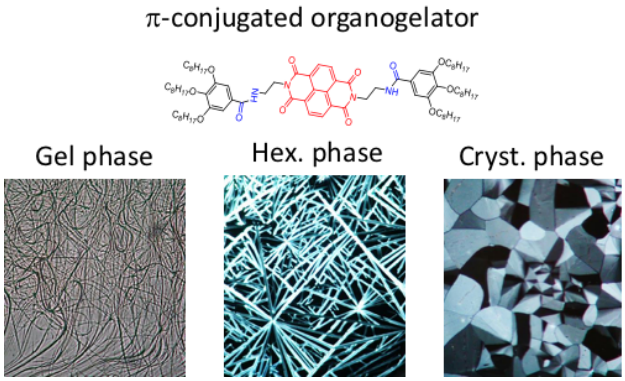

## I. Introduction.

Rylene bisimides form a unique and interesting class of organic semiconductors widely used in the community of plastic electronics.[1-3] Rylene bisimides such as perylene and naphthalene bisimides are robust and versatile polycyclic building blocks that can be used for the synthesis of new molecular and polymer semiconductors with interesting electronic properties e.g. n-type charge transport in OFETs[4-7] or high luminescence of interest for sensor application.[8-10] Their excellent thermal and oxidative stability as well as high electron affinities are readily exploited to design n-type semiconductors with high charge mobilities > 0.5 $cm^2/V{\cdot}s$.[11,12] The electronic and optical properties of individual rylene bisimide molecules can be tuned by molecular engineering and adequate choice of substituents.[3,13-16] However, their collective properties in the solid state depend on molecular packing. For instance, they can form different polymorphs made of either J- or H-type aggregates, as observed for perylene bisimide (PBI) derivatives.[17-19] In PBI-based organogelators, the competition between H-bonding and π - π stacking interactions determines the organization in the supramolecular assemblies, hence the electronic properties in the solid state.[20,21] Depending on the lateral substituents, perylene and naphthalene bisimides can form a large variety of structures in the solid state e.g. crystalline and liquid crystalline phases, and can also form physical gels in organic solvents. While gelation of π-conjugated systems involving rylene bisimides has been described in the literature,[22] the structures formed in the gels are only marginally described. In most cases, the fibrilar aggregates formed upon gelation are made of columnar or helical supramolecular stacks driven by H-bonding interactions.[23-25] However, at the same time, organogelators are also subject to polymorphism and the structures formed in organic solvents may transform to different supramolecular arrangements when the films are subjected to thermal annealing after drying of the gel for instance. As an example, a PBI-based organogelator similar in molecular

structure to NDI2 (see Figure 1) forms fibrillar J-type aggregates in the dried gel that transform to H-type aggregates upon thermal annealing.[20] The PBI-analogue of NDI2 can thus be converted from a columnar structure in the dried gel to a hexagonal frustrated trigonal structure made of $2_1 1$ supramolecular helices.[21] Interestingly, exposure of the H-aggregate phase to vapors of H-bonding non solvents (acetone or ethanol) converts the film back to the J-aggregate columnar phase. Therefore, the polymorphism of organogelators based on rylene bisimide can be used to design stimuli-responsive materials.[21,20] Moreover, association of PBI-based semiconductors and electron donor polymers such as P3HT can lead to interesting nanostructured shish-kebab morphologies of potential interest for photovoltaic applications.[26]

In this manuscript, we focus on NDI2 (see Figure 1.a). Ghosh et al. reported the gelation of this compound and proposed a columnar stacking based on H-bonding between amides of successive molecules without structural evidence.[15] Herein, the full phase diagram of NDI2 in the solid state is proposed, with the description of four structural variations including the gel phase (form I) and three solid state phases. The first part of this study is dedicated to the gelation of NDI2 in *trans*-decaline (TD) including the structure of the dried gel phase. The second part of the study focuses on the different polymorphs of NDI2 in thin films identified and characterized by DSC, UV-vis/FTIR spectroscopy and low dose TEM (HR-TEM and electron diffraction). A structural model is determined from electron diffraction analysis for the metastable LC phase (form II) made of $6_1$ supramolecular helices. Most interestingly, single crystal X-ray diffraction helped determine the exact packing of NDI2 molecules in the crystalline form (form IV). Finally, a complete phase diagram explains how the polymorphs are interconverted.

## II. Experimental section.

### a) Synthesis.

NDI-2 (N,N'-di(1-(3,4,5-tri(octyloxy)benzamido))eth-1yl naphthalene-1,4,5,8 tetracarboxylic acid bisimide) was synthesized according to the synthetic method described in the ref 21,22, or with a modified procedure described in details in the SI section. All solvents used to prepare the gels from solution were used as received except *trans*-decaline, filtered on a column of $Al_2O_3$.

### b) Preparation of NDI2 polymorphs.

Thin films of the different NDI2 polymorphs were prepared from amorphous films prepared by casting 50 µl of solution in chloroform (1 mg/ml) on either glass substrate or oriented poly(tetrafluoroethylene) (PTFE) substrates. Solvent vapor annealing (SVA) in chloroform afforded form I of NDI2. For SVA, the films were placed in a closed glass container filled with 5 ml of chloroform at room temperature for 1 day. The form II (IV) was obtained by annealing the cast films for 30s (Linkam hot stage under $N_2$ atmosphere) at 240°C (200°C). After annealing, the samples were cooled to room temperature at a rate of 10 °C/min.

Oriented poly(tetrafluoroethylene) (PTFE) substrates are particularly well suited for the alignment of polymers and molecular materials. They were prepared by friction transfer on clean glass substrates following the protocol described in reference 27.

### b) Structural characterization.

The polymorphs of NDI2 were identified under the Polarized Optical Microscope (POM) on a Leica DMR-X microscope (equipped with a Nikon Coolpix 995 digital camera) in phase contrast or under crossed polarizers. *In situ* temperature annealing experiments were

carried out in the POM at a rate of 50°C/min for both heating and cooling ramps using a Linkam LTS 420 heating plate.

Transmission electron microscopy was performed on a Philips CM 12 (120 keV) microscope equipped with a CCD MVIII digital camera. The observations were performed in bright field, high resolution and electron diffraction modes. Low dose exposure conditions were used to avoid sample damaging by the electron beam. The rotation-tilt experiments were carried out using a Phillips PW6594 sample holder. The in situ temperature annealing experiments were carried out with a gatan single tilt heating holder and a smart set 901 hot stage controller. For TEM investigations, the NDI2 films were coated with a thin amorphous carbon film, removed from the glass substrate by using polyacrylic acid, subsequently floated on distilled water and recovered on TEM copper grids. For studies of the fibers in the gel phase, droplets of the solution were directly cast on carbon coated TEM grids and the solvent was left to evaporate. For the structural investigation on the crystalline form IV in thin films, oriented NDI2 films were prepared by casting a solution in chloroform on an oriented PTFE substrate. Thermal annealing at 220°C, yielded oriented crystals of form IV on the PTFE substrate.

Image treatments were carried out using AnalySYS (Soft Imaging Systems). The structural modeling and the calculation of electron diffraction patterns were performed using the proper modules of the Cerius2 Software on a SiliconGraphics Octane workstation.

For AFM imaging, NDI2 solutions were cast on clean silicon wafers. The observations were made in peak force tapping mode on a Bruker Multimode controlled by a Nanoscope V module with a *Si3N4 tip* with a constant of 0.4 N/m and a terminal radius below 5 nm oscillating at a frequency between 250 and 300 kHz. The image treatment was carried out using Nanoscope Analysis software.

The powder diffraction patterns were obtained with a transmission Guinier-like geometry. A linear focalized monochromatic Cu Kα1 beam ($\lambda = 1.5405$ Å) was obtained using

a sealed-tube generator equipped with a bent quartz monochromator and diffraction patterns were recorded with a curved Inel CPS120 counter gas-filled detector, from samples filled in Lindemann capillaries of 1 mm diameter. The TREOR program was used to index the peaks of the powder diffraction patterns and extract a unit cell (form I).

X-Ray diffraction data collection was carried out on a Bruker APEX II DUO Kappa-CCD diffractometer equipped with an Oxford Cryosystem liquid $N_2$ device, using Cu-Kα radiation (λ = 1.54178 Å). The crystal-detector distance was 40 mm. The cell parameters were determined (APEX2 software)[29] from reflections taken from three sets of 20 frames, each at 10 s exposure. The structure was solved by direct methods with the program SHELXS-2013.[30] The refinement and all further calculations were carried out using SHELXL-2013.[30] The hydrogen H2N was located from Fourier difference maps and refined isotropically. The other H-atoms were included in calculated positions and treated as riding atoms using SHELXL default parameters. The non-H atoms were refined anisotropically, using weighted full-matrix least-squares on F2. A semi-empirical absorption correction was applied using SADABS in APEX2;[30] transmission factors: $T_{min}/T_{max}$ = 0.6385/0.7528. The atoms C23 and C24 are disordered over two positions with an occupancy ratio of 0.6/0.4.

**c) Spectroscopy (UV-vis and FTIR).**

UV-Visible spectroscopy was performed on an Agilent Cary 5000 spectrometer with a resolution of 0.5 nm. The *in situ* temperature annealing experiments were carried out at a rate of 50 °C/min for both heating and cooling ramps using a Linkam LTS 420 heating plate fitted inside the sample chamber of the spectrometer. The spectra were measured every 10 °C after holding the temperature during 1min under $N_2$ flow.

The FTIR spectra were measured with a Bruker Vertex 70 spectrophotometer in transmission mode. The spectra were measured with a resolution of 2 $cm^{-1}$ and accumulation

of 64 scans. The films of Form I were obtained on a NaCl plate by drop casting from a solution in chloroform (1 mg/mL) then by solvent vapor annealing treatment with chloroform in a dessicator. The Form II and III films were obtained by annealing films on NaCl in a Linkam heating stage under nitrogen at 240°C and 200°C respectively for 30 s and quenched at room temperature. The *in situ* temperature annealing experiments were carried out at a rate of 50 °C/min for both heating and cooling ramps using a Linkam LTS 420 heating plate fitted inside the sample chamber of the spectrometer. The spectra were measured every 5 °C after holding the temperature during 2 min.

The DSC measurements were performed with a PerkinElmer DSC 8500. The TGA measurements were performed with a Mettler TG50 microscale and a Mettler TC10A controller. For these experiments, the powders were placed in alumina crucibles under $N_2$ and temperature was increased at 10 °C/min.

## III. Results and discussion.

### a) Gel phase.

Because of the presence of amide groups, NDI2 forms gels in organic solvents. The formation of NDI2 gels has been first verified visually for a number of solvents listed in table S1. Gels are formed in solvents such as *p*-xylene, cyclohexane and *trans*-decaline (TD) whereas in acetone or alcohols, NDI2 precipitates. In chloroform, NDI2 forms no gel and is soluble even for high concentrations up to 15 mg/ml. UV-vis spectroscopy has been used to determine the different spectroscopic signatures of the gel and sol phases (Fig. 1b). The spectrum of non-aggregated NDI2, at high temperature, shows a vibronic structure with maxima at 378, 358 and 342 nm. Upon gelation, the spectrum is slightly red-shifted by 7 nm but without broadening of

the vibronic structure. Most characteristic of gelation is the change in the intensity ratio of the 0-0 and 0-1 components of the vibronic structure of the NDI core. It is thus possible to characterize the gel→sol transition of NDI2 in TD as a function of temperature by following the temperature dependence of the ratio, $A_{0\text{-}0}/A_{0\text{-}1}$ where $A_{0\text{-}0}$ and $A_{0\text{-}1}$ are the amplitudes of the 0-0 and 0-1 components in absorption. The evolution of both the UV-vis spectrum and of the $A_{0\text{-}0}/A_{0\text{-}1}$ ratio *versus* temperature are shown in Figure 1.b and 1.c, respectively. To perform the experiment, for each temperature step, the sample was allowed to reach an equilibrium state after 30 min i.e. such that no evolution of the spectrum was evidenced. With this procedure, kinetic effects on the aggregation process upon cooling were avoided. The ratio $A_{0\text{-}0}/A_{0\text{-}1}$ shows a reversible and sharp change with temperature as seen in Figure 1.b. In the sol phase, the ratio $A_{0\text{-}0}/A_{0\text{-}1}$ is strictly larger than unity whereas in the gel phase it is below unity. Interestingly, the curves for the T-dependence of the ratio overlap perfectly upon heating and cooling, indicating that the transition is reversible. A transition temperature of 110 °C for $1x10^{-3}$ M can thus be extracted from the UV-vis study for the gelation of NDI2 in TD (inflection point in the graph of $A_{0\text{-}0}/A_{0\text{-}1}$ *versus* temperature in Figure 1.c). The same experiments at different concentrations of NDI2 afford the phase diagram of NDI2 in TD showed in Figure 1.d. As observed for most π-gels, the gel→sol transition temperature tends to increase with increasing concentration of the solution but without reaching a plateau. The overall phase diagram is consistent with the phase diagrams of NDI2 obtained from DSC in different solvents.[15]

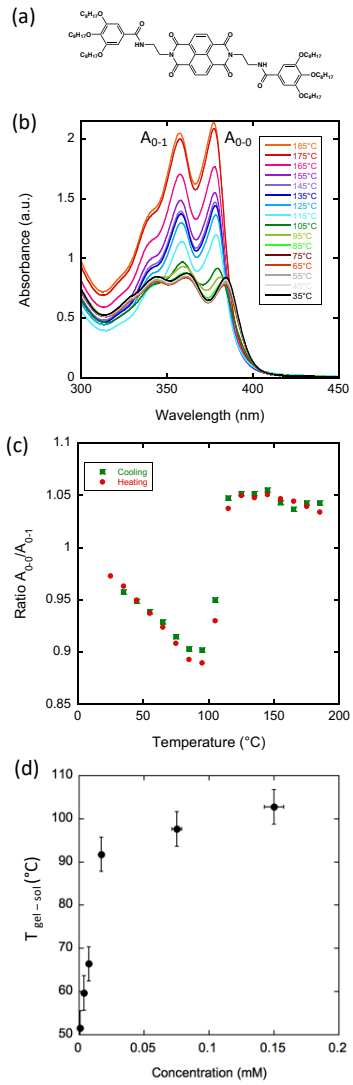


**Figure 1**. (a) Chemical structure of NDI2. (b) Evolution of the UV-vis absorption spectrum of NDI2 in TD (0.15 wt %) as a function of temperature, starting from the gel phase at room temperature. (c) Evolution of the $A_{0\text{-}0}/A_{0\text{-}1}$ ratio upon heating and cooling of the gel (c=0.15 wt % in TD). (d) Concentration-temperature phase diagram of NDI2 in TD as obtained from UV-vis analysis showing the dependence of the temperature of gel → sol transition, $T_{gel\text{ - }sol}$ with concentration in TD.

The structure and the morphology of the dried gel were analyzed by AFM and TEM to determine the type of assembly of the NDI2 molecules in the gel phase. As seen in Figure

2.a, very long fibers, tens of microns in length, are formed by gelation in TD. These fibers show only limited birefringence in POM and therefore, they can be identified only in phase contrast in optical microscopy. The poor birefringence suggests limited crystallinity. Electron diffraction performed on a bundle of fibers (see Figure 3) shows two reflections at 4.8 Å and 29.7 Å corresponding to the inter-molecular distance between NDI2 molecules in the columns and the inter-columnar distance, respectively. The 4.8 Å repeat period is characteristic of H-bonded amides. It is oriented along the long fiber axis, which indicates that the fiber long axis corresponds to the direction of H-bonding.[31] Therefore, the fast growth direction of NDI2 fibers corresponds to the H-bonding direction between amides. The columnar arrangement of NDI2 molecules is further ascertained by low dose HRTEM showing periodic fringes with 30 Å periodicity. The contrast in HRTEM images is attributed to the difference in the electronic density between the aromatic core and the adjacent layers of alkyl side chains.

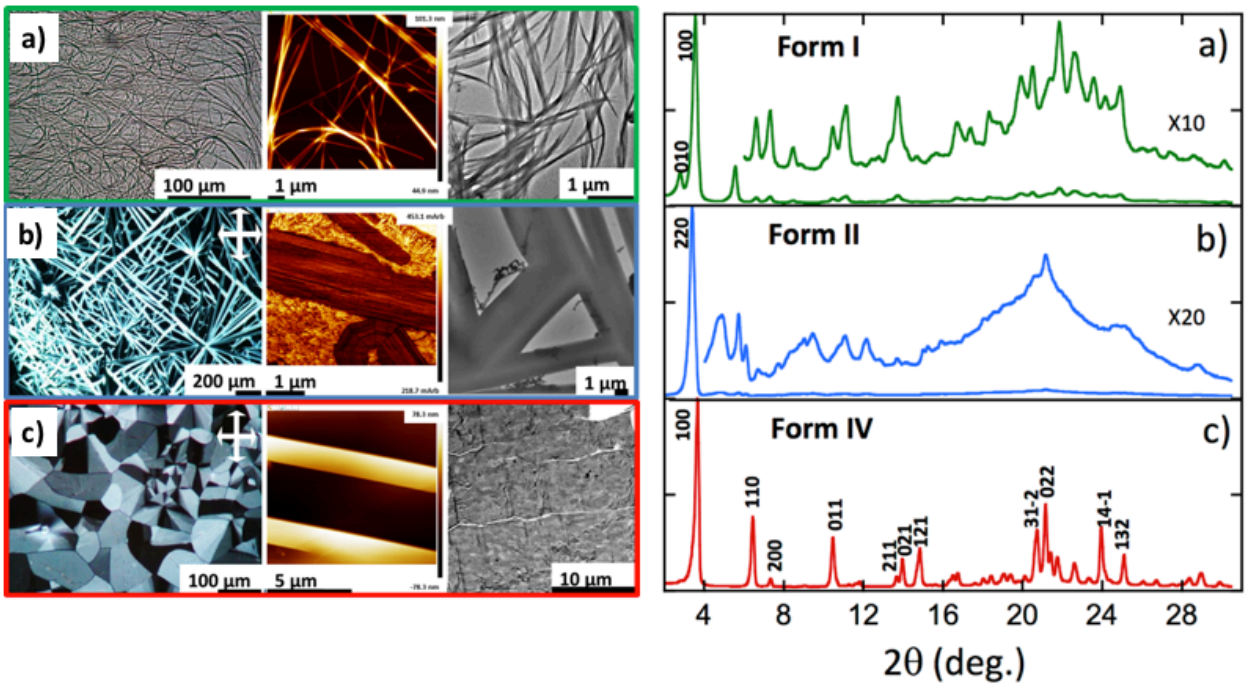


***Figure 2.*** *Morphology and structure of three polymorphs of NDI2. (a) Form I (green), (b) Form II (blue) and (c) IV (red) of NDI2. From left to right: Morphology as observed by optical*

*microscopy, Atomic force microscopy (AFM) and bright Field TEM, X-ray powder diffractogram. Note that the AFM image for form II in (b) corresponds to a phase mode image whereas topography mode images are shown for other polymorphs. Due to the very weak birefringence of form I, the optical microscopy image showing long fibers of form I in (a) corresponds to phase contrast.*

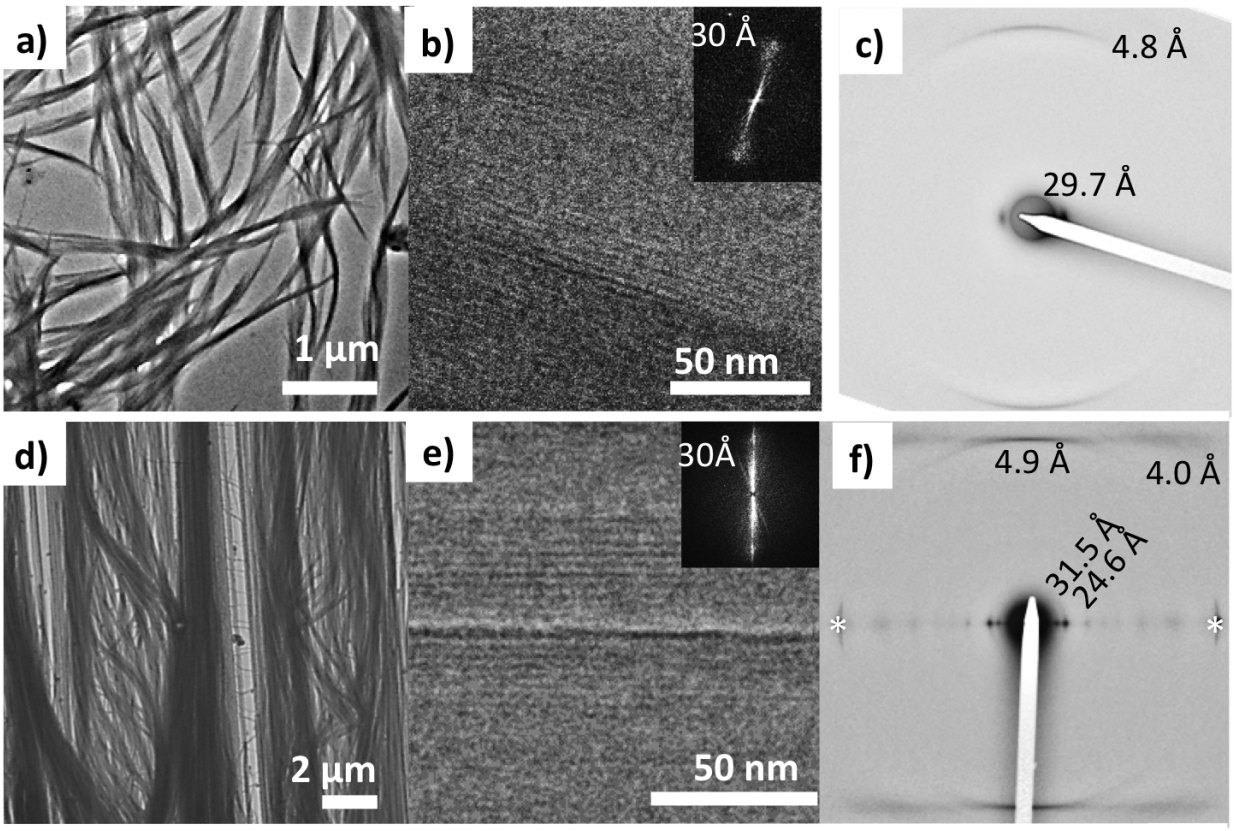


***Figure 3**. (a-c): Fibrillar morphology of NDI2 dried gel phase. (a) Bright Field, (b) HRTEM with corresponding FFT, (c) electron diffraction pattern. (d-f) Morphology of oriented NDI2 films obtained by SVA in $CHCl_3$ on oriented PTFE substrates. (d) Bright field, (e) HRTEM with corresponding FFT, (f) electron diffraction pattern. The asterisk points at the 100 reflection of the oriented PTFE substrate (4.9 Å) used as a reference to calculate reticular distances.*

To gain more insight in the structure of the gel phase (form I), attempts were made to orient this phase in thin films. Incidentally, an amorphous-like film of NDI2 (cast from chloroform solution) subjected to solvent vapor annealing (SVA) in chloroform vapors (several hours) yields the same fibrillar structures as for the dried gel phase (form I) and shows the same UV-vis spectrum. When the same preparation protocol is used on oriented PTFE substrates, NDI2 fibrils grow parallel to the PTFE substrate (see Figure 3). TEM analysis of the aligned films gives evidence for a columnar-phase with H-bonding directed along the fiber long axis. The electron diffraction of aligned fibers of NDI2 shows the same reflections as the dried gel as well as additional reflections at 24.6 Å and 4.0 Å. The HRTEM images reveal the same columnar stacking with a 30 Å repeat period as observed in the dried gel. Accordingly, the dried gel and the oriented films prepared by SVA in chloroform correspond to the same polymorph (form I).

This structure is further ascertained by a powder X-ray diffraction analysis on powder samples prepared by SVA in $CHCl_3$. Figure 2.b shows the characteristic powder X-ray diffractogram of form I. The diffractogram of this form is strictly distinct from that of the other polymorphs, showing no common diffraction peaks (indicative of a pure phase). The most important diffraction peaks at 24.3 Å and 31.6 Å are close to those observed by ED for the oriented fibers on PTFE substrates. This diffraction pattern was indexed, yielding a monoclinic unit cell: a=24.3Å, b=32.3Å, c=9.87Å, β=97.0° and Z=4. The c axis corresponds to the H-bonding direction of the NDI2 molecules, it is twice the H-bonding period of 4.8-4.9 Å measured in the fibers in the dried gel. This implies that the two molecules along the c axis are related by a symmetry element, possibly a $2_1$ axis given the systematic absence of the h k 1 reflections in the ED pattern of oriented fibers. The unit cell parameters suggest a columnar arrangement.

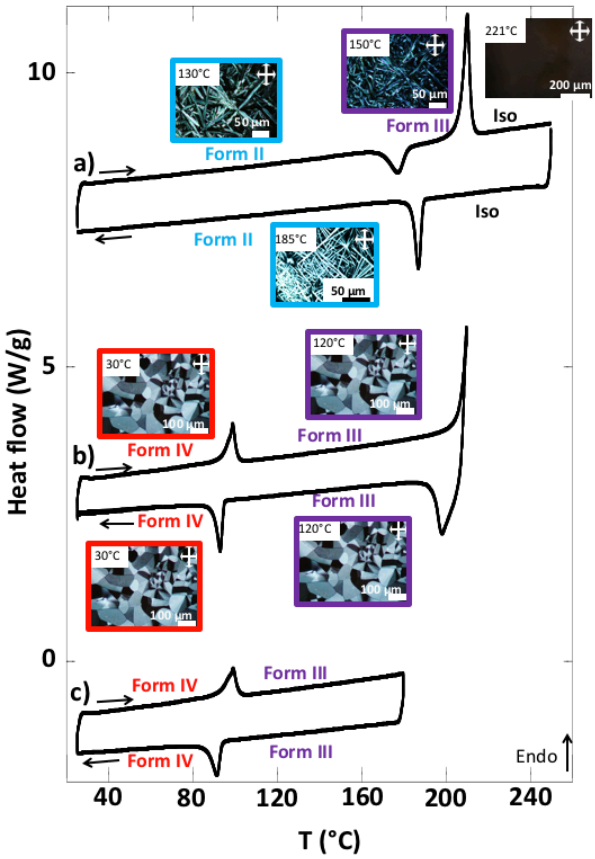


***Figure 4.*** *Differential Scanning Calorimetry diagrams of NDI2 between 25°C to 250°C at a rate of 10°C/min. Three scans are shown and correspond to different temperature ranges. In (a), the sample is annealed well above the melting temperature and the metastable form II is obtained after cooling. To start from the form II, the heating trace was measured during the second heating cycle. In (b), the heating is performed up to the maximum of the melting peak and only the form III followed by form IV are obtained upon cooling. Finally in (c), the sample is heated at a temperature below the melting and thus the isotropic phase is not attained. The DSC trace shows only the form IV → form III reversible transition due to alkyl side chain melting/crystallization. The insets correspond to the POM images of the various phases.*

**b. Metastable LC phase (form II) and crystalline/lamellar phase (IV, III).**

Beside the dried gel phase, DSC and POM evidence three additional polymorphs. Figure 2 depicts the morphologies and the X-ray diffractograms of the polymorphs observed in the solid state whereas Table S2 collects the transition temperatures between the different phases. Starting from the dried gel phase or a cast film, large and highly birefringent spherulites (form IV) are generated by thermal annealing at T>170 °C (see Figure 2.e). TEM indicates that these spherulites consist of a crystalline phase (see Figure 5). Rotation-tilt experiments on thin films oriented on PTFE substrates allowed to extract a first estimate of the unit cell parameters for form III: a=24.2 Å, b=16.3 Å, c=10.1 Å and β=99.6°. This unit cell is further ascertained by single crystal analysis (vide infra).

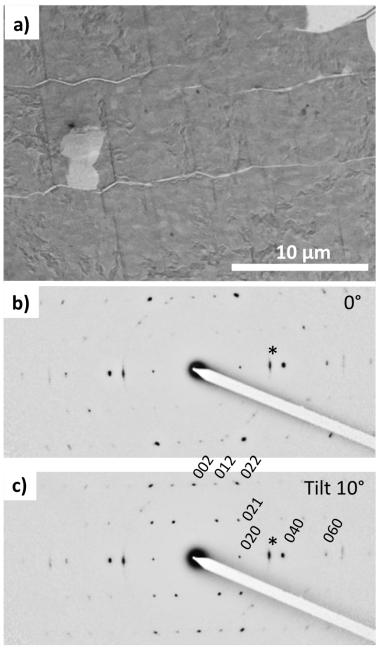


***Figure 5****. Morphology of a form IV thin film of NDI2 oriented on PTFE. a) Bright field, b) diffraction pattern and c) diffraction pattern obtained for a 10° tilt around the b* axis. The asterisk points at the 100 reflection of the PTFE substrate.*

Spherulites (Form IV) melt at 210 °C (POM) (see DSC trace in Figure 4 b-c and Table S2) but below, at 99°C, an endothermic transition is observed upon heating . This transition is reversible : an exothermic peak is observed at 93 °C upon cooling. Its enthalpy, 24-28 kJ/mol, is consistent with the melting of crystallized alkyl side chains. Therefore, at low temperature a crystalline form is obtained (form IV, Cr.) which transforms to a lamellar phase (form III, Lam.) upon melting of alkyl side chains at 99 °C. This result is further supported by in situ TEM and by FTIR spectroscopy as a function of temperature (see Figure S1 and S2).

Beside the crystalline and lamellar phases, a fourth phase is observed. When, form IV is molten at 220 °C, the same crystalline phase is formed upon cooling back to RT. However, if the form IV is heated to 240-250 °C, a different phase (form II) is obtained upon cooling. Form II consists of long and strongly birefringent needle-shaped crystals (Figure 2.b) very different from the spherulite-like morphology of form III and IV. The diffractogram of form II is distinct from those of the spherulites and of the dried gel phase (Figure 2.a and 2.c), demonstrating the formation of a different and pure phase (form II). Moreover, as seen in Figure 4, the DSC trace indicates that this phase transforms back to the lamellar phase (form III) when heated to 157 °C (as indicated by the exotherm in the second heating scan shown in Figure 4) and finally to the crystalline form IV when cooled back to RT. This result ascertains that form II is not related to a degradation of NDI2. The limited set of reflections in form II (see Figure 2) points at a liquid crystalline phase (columnar phase), which is further confirmed by TEM (vide infra). Accordingly, form II is considered as a quenched LC phase obtained upon cooling from the isotropic melt heated at T≥240 °C.

The existence of two different phases formed upon cooling from a “molten phase” at different melt temperatures is original. A tentative explanation can be given based on the crystal structure of form IV (vide infra). We postulate that, in order to obtain the LC form II, it is necessary to fully suppress the nuclei of form IV that are particularly stable (see structure of

form IV as described below). Such nuclei may involve only a couple of molecules linked by H-bonding as well as π-stacking between phenyl groups and NDI. The presence of some residual H-bonds in the melt phase, is consistent with FTIR results showing that some amides are still involved in weak H-bonds (vide infra).

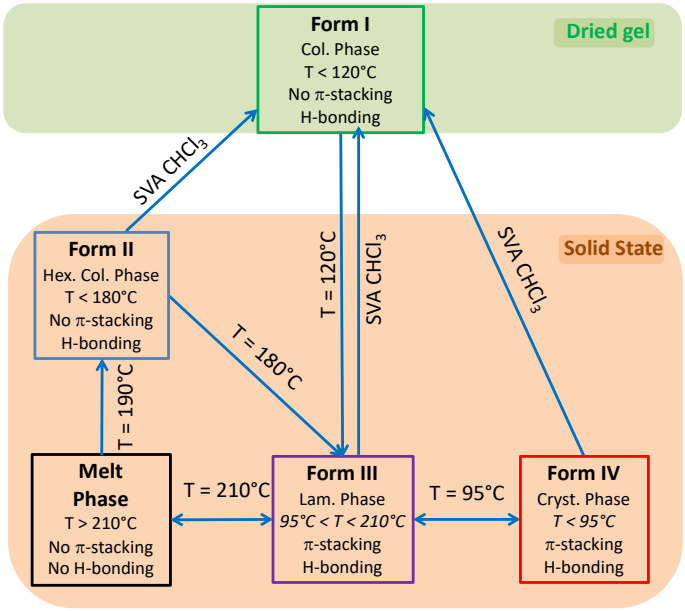


**Figure 6**. Phase diagram of NDI2 in the solid state showing the means to obtain four polymorphs: form I (gel phase) made of fibrils, form II (quenched and metastable LC phase), form III (lamellar phase) and form IV (crystalline phase yielding spherulites in thin films).

To summarize, Figure 6 illustrates the solid state phase diagram of NDI2. This diagram shows the different ways to interconvert the four identified polymorphs of NDI2. As such, the polymorphism of this organogelator is very complex and is seldom observed for similar compounds.

### b) Spectroscopic signatures of the polymorphs of NDI2.

The UV-vis and FTIR spectra of the polymorphs I, II and IV were measured at RT, those of the polymorph III at 110 °C (it exists only between 95 °C and 210 °C). UV-vis spectroscopy

identifies π-stacking by the broadening and shifting of absorption features accompanying molecules association. FTIR spectroscopy helps determine the strength of H-bonds by following e.g. the $\nu_{NH}$ bands of the amides.

First, the dried gel (form I) and the form I fibers obtained in *trans*-decaline (TD) show a vibronic structure similar to that of the dissociated NDI2 molecules in chloroform. The main 0-0 and 0-1 peak positions are only slightly blue shifted (from 382 nm in $CHCl_3$ to 385 nm for form I). This suggests marginal π-overlaps between NDI units in form I (dried gel and fibers in TD). The UV-vis spectrum of form II is also a vibronic structure similar to that of dissociated NDI2 molecules in $CHCl_3$ i.e. typical of marginal π-stacking. The UV-vis spectrum of form III and IV are very different and consist of two broad bands centered at 362 and 375 nm. In a NDI derivative such as N,N'-bis[6-hexyl-3,4,5-tridodecyloxybenzester]naphthalene-1,4,5,8-tetracarboxyl-bisimide,[32] such broad absorption spectrum was also evidenced and due to the strong orbital overlaps between NDI molecules in the unit cell. This result suggests that NDI molecules show stronger π-interactions in form IV and III than in form I and II. However, as shown hereafter, the π-overlaps involved in the form III and IV are between NDI and phenyl rings of neighboring NDI2 molecules and not between π-stacked NDIs.

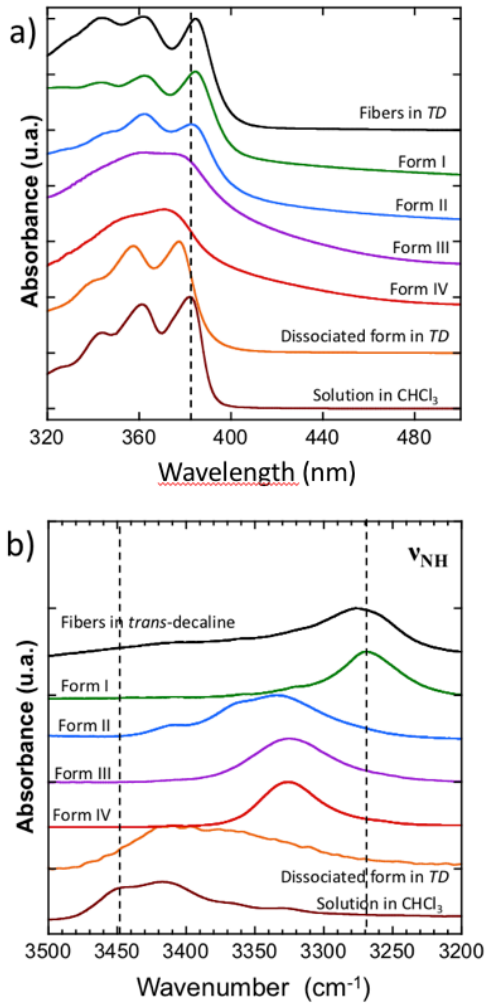


**Figure 7.** (a) UV-Vis spectra of the four polymorphs of NDI2 and in solution in chloroform and in *trans*-decaline (TD). The dissociated form in TD is obtained at T=120 °C. (b) FTIR spectra (thin films) of the four polymorphs of NDI2, the melt and the solutions in TD. In both plots, the successive spectra were offset along the ordinate axis for clarity.

Further differences between polymorphs are observed in the FTIR spectra around 3200-3500 $cm^{-1}$ that features the characteristic amide band(s) ($\nu_{NH}$ stretching) (Figure 7.b). The position of this band reflects the intensity of H-bonds: it shifts to lower energies when the intensity of H-bonding increases.[33,34] As seen in Figure 7, the gel phase (form I) shows the amide band with lowest energy at 3269 $cm^{-1}$, proving that H-bonds are the strongest in this

polymorph. The form II is a mesophase and it shows a structured band composed of at least three components at 3333, 3360, 3410 $cm^{-1}$. The latter component has a position close to that observed in the melt where no H-bonds are present, suggesting the presence of a fraction of non-bonded amides in the form II mesophase. The presence of different populations of amides with different H-bonding intensities is consistent with the picture of a LC phase containing structural disorder in the stacking of NDI2 molecules. Most importantly, in the crystalline structure (IV), the NH stretching band is seen at 3325 $cm^{-1}$, a position indicating weaker H-bonds than in the gel phase (form I). But despite weaker H-bonds in form IV, DSC shows that form IV is the thermodynamically stable phase, not form I. Concerning the comparison of form III and IV, the FTIR spectra indicate identical peak positions. The only visible differences concern the frequencies of the $\nu_{CH2}$ bands (see Figure S2). The asymmetric stretching band shifts from 2921 $cm^{-1}$ in the crystalline phase (form IV) to 2926 $cm^{-1}$ in the lamellar phase (form III). This shift shows that the alkyl chain are crystallized in form IV, and disordered in form III. Indeed the lower frequency indicates alkyl chains in all-*trans* conformation, and this frequency increases with the ratio of gauche/trans conformations in the chains.[34,35]

**d) Structural model for the quenched LC phase.**

The XRD pattern obtained for form II indicates a columnar mesophase but is unable to give further structural information on the molecular assemblies except a possible intra-columnar repeat of 4.2 Å from the peak around 21.2° (see Figure 2.d). Therefore, thin oriented films of form II were prepared on oriented substrates of PTFE to analyze the structure by electron diffraction. Upon melting and recrystallization, highly oriented needles of form II are readily oriented on PTFE. Figure 8 shows the typical ED pattern for such oriented films. First, this pattern reveals a remarkable level of organization that could not be inferred from the powder XRD pattern. This pattern consists of a set of layer lines on which reflections are localized. The layer lines are perpendicular to the long axis of the form II needles. Strong reflections are

observed on the 1st, 5th, 6th and 7th layer lines (see schematic illustration 8.b). The first meridional reflection is located on the 6th layer line. This indicates that NDI2 self-assembles into $6_1$ helices with the helix axis parallel to the PTFE chain direction. Indeed, in the diffraction pattern of a $6_1$ helical structure the reflections are located on layer lines with index l defined as l=6m±n where m and n are integers.[37-39] The stacking period between NDI2 molecules is p=3.6 Å whereas the helical long period P=21.6 Å. This means that successive layers of NDI2 molecules in the helices are rotated by 60° around the helical axis. The fact that rylene-based molecules can form such helical assemblies has been demonstrated previously for perylenebisimide derivatives by circular dichroism measurements and electron diffraction.[25,21] Recently, a PBI derivative similar to NDI2 showed the formation of $21_1$ supramolecular helices.[21] In the ED pattern in Figure 8.a the reflections of the 5th, 6th and 7th layer lines are streaked in the direction perpendicular to the helical axis. This streaking proves structural disorder between adjacent helices, in agreement with the liquid crystalline character of form II. Further evidence of helical assemblies was obtained by HRTEM. As seen in Figure S3, regular fringed ED patterns are observed by HRTEM when the films are tilted at ±30° around the helical axis (PTFE chain direction) but not at 0° tilt. The period for the HRTEM image equals 26 Å and is identical to the inter-columnar period observed by XRD and by electron diffraction. In addition, the rotation-tilt experiment also shows that the intensity of the 26 Å peak is maximum for ±30° tilt around the column axis. Both these observations demonstrate that the helices are packed in a trigonal unit cell.

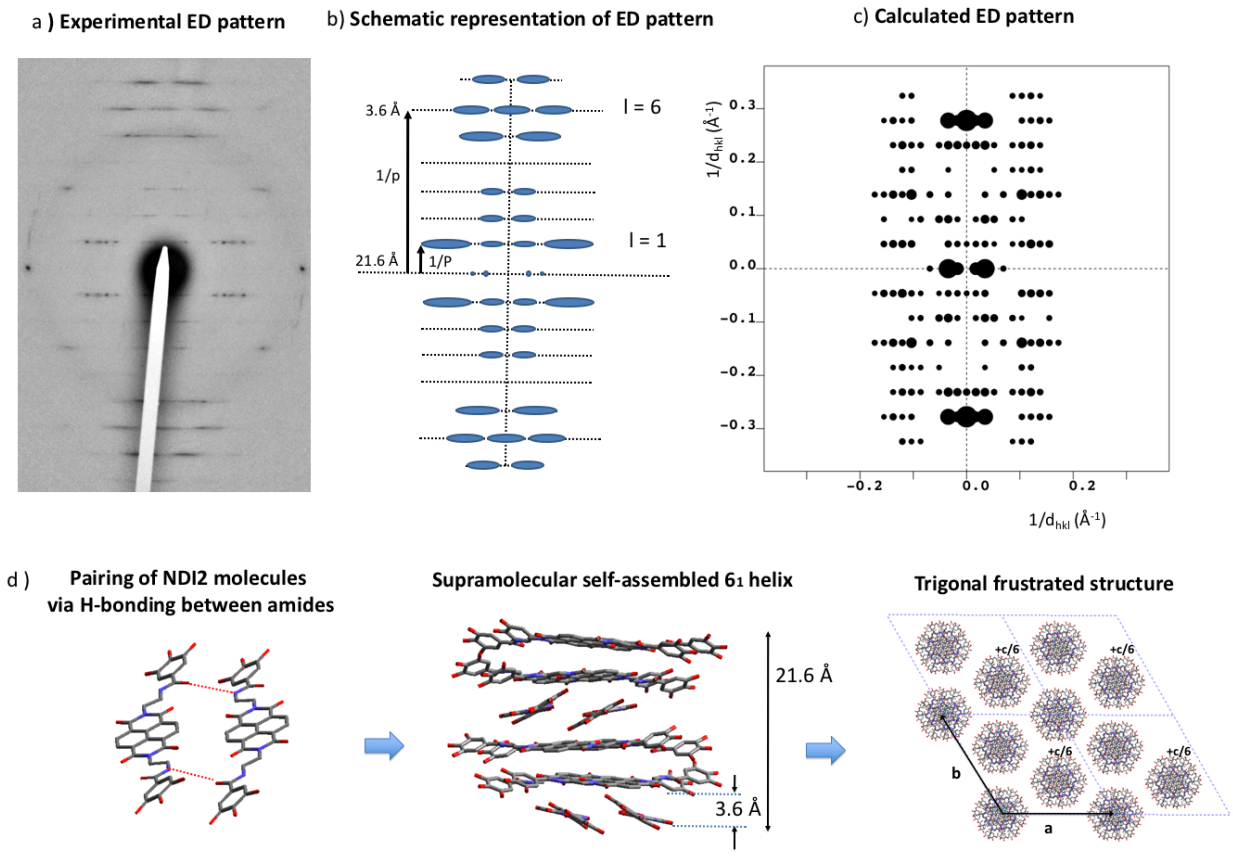


***Figure 8***. *Electron diffraction pattern of a single needle of form II of NDI2 (LC phase). (a) experimental electron diffraction pattern, (b) schematic representation of the pattern and (c) calculated ED pattern . (d) Structural model showing the pairing of NDI2 molecules via H-bonding between amides in the dimer, the supramolecular helical assembly and the trigonal unit cell formed by three 6₁ helices of NDI2. The helices are ex-centered, have a long period of 21.6Å and a residue of 3.6 Å. Note that one helix over three is shifted by c/6 along the c axis (helix axis) of the unit cell as expected for frustrated trigonal structures.*

Despite the structural disorder in form II, the helical columnar phase of NDI2 was modeled based on the ED pattern in Figure 8.a. As shown by Percec and coworkers, analogous PBI-based molecules show similar helical assemblies.[40,41] The supramolecular assemblies are made of dimers that stack along the helical axis. The core of these helices contains the conjugated

macrocycles (PBI, or NDI in the present case) whereas the mesogen groups form the disordered corona of the helices. The same packing was recently uncovered in the case of a PBI analogue of NDI2 by Sarbu et al.[21] In the case of NDI2, a supramolecular helical assembly has been constructed from "dimers" of NDI2 molecules linked together by H-bonds as shown in Figure 8.d. In such an assembly, H-bonds are supposed to be formed only within the dimers and not between layers of dimers in the helices. This assumption is supported by the fact that the distance between NDI2 dimers along the helical axis is typical of π-stacking (3.6 Å) whereas in form I and IV, the repeat period between H-bonded NDI2 is typical of H-bonding between amides i.e. 4.8-4.9 Å. In the dimers shown in Figure 8.d, not all the amides of the NDI2 molecules are linked by H-bonds. This is consistent with the FTIR analysis of form III that has shown the coexistence of different populations of amides with different H-bonding strengths.

When constructing a helical assembly using such H-bonded dimers, the barycenter of each dimer can be located either on the helical axis or ex-centered. The distance from the dimer barycenter to the helical axis was used as a variable in our calculations of the ED patterns of the helices, following the same approach as proposed previously by Sarbu et al.[21] In a first approximation, the ED pattern was calculated for a trigonal unit cell containing a single helix (a=b=30 Å, c=21.6 Å and γ=120°), to verify if the intensities in the various layer lines can be properly reproduced. As a matter of fact, only ex-centered helical assemblies reproduce correctly the intensities in the $1^{st}$, $5^{th}$, $6^{th}$ and $7^{th}$ strata of the experimental ED pattern. A radius of 1.5 Å was found optimum. Ex-centering the dimers results in a reduced π-stacking between NDI cores in the helices which is consistent with the marginal broadening and shifts of the UV-vis absorption bands in form II. A single helix unit cell is however unsatisfactory as the resulting packing density is not consistent (form IV shows a density of 1.16 g/cm$^3$). As proposed in our recent study on a PBI-analogue of NDI2, three helices of NDI2 molecules are associated in a triplet in a trigonal unit cell. A crystal density of 1.18 g/cm$^3$ is obtained for a

trigonal unit cell with a=b=58±2 Å, c=21.6 Å and γ=120°. Such a large unit cell is further supported by the repeat period between reflections in the 1st layer line of the ED pattern that yield a unit cell parameter a= 58±2 Å (see Figure 8.a). The final calculated ED pattern for this structural model is shown in Figure 8.c. This pattern corresponds to a unique zone axis and accounts well for the distribution of dominant reflections in the main layer lines. However, some discrepancy is evidenced for the intensities in the 6th layer line with a strong overestimation for the meridional reflections. Indeed, the structural model does not take into account the packing disorder inherent to LC phases. As seen in Figure 5.a, disorder in the packing of NDI2 columns i.e. random offsets between columns along the c axis results in the streaking of the reflections in the 5th, 6th and 7th strata. Such a streaking implies a redistribution of the intensities of the reflections in the 6th strata, and explains, at least in part, why the measured intensities in the 6th layer are lower than the calculated intensities.

**e) Crystal structure of form IV and III.**

Crystallization of NDI2 in a mixture of methanol/chloroform afforded single crystals of form IV that were subjected to X-ray diffraction analysis. It has been verified that the structure of the single crystals is identical to the structure observed in the films showing large spherulites. The experimental ED pattern in thin films can be perfectly accounted for by the calculated ED pattern for the [100] zone using the single crystal structure (see Figure S1). Figure 9 shows some characteristic projections of the refined crystal structure. The obtained molecular packing of NDI2 in form IV is far from the "expected" packing for such molecules, based on long-range π-stacking of the NDI cores. In form IV, NDI cores do not π-stack together and cannot form columnar stacks. Most surprisingly, each NDI is π-stacked between the phenyl groups of two dendrons belonging to two adjacent NDI2 molecules (Figure 9.b). This π-

stacking interaction between NDI and phenyl groups accounts for the shift and the broadened UV-vis absorption spectrum of form IV as compared to form I and II. In addition, the organization of NDI-C8 is hinged on intermolecular H-bonds between amides. The H-bonds are along the **c** axis of the unit cell (see Figure 9). Only one population of H-bonded amides is present in this structure, in agreement with the IR results showing a single amide band at 3325 $cm^{-1}$. As shown by The projection along the **c** axis in Figure 9.c, the structure alternates layers of interdigitated alkyl side chains and layers of π-stacked phenyl/NDI/phenyl. The form III obtained by heating form IV at a temperature above 99 °C corresponds to the same structure with H-bonded amides but with molten alkyl side chains. Temperature-dependent TEM demonstrates that the core of the structure is identical in form III and IV. As seen in Figure S1, the intensities of the dominant reflections in the ED pattern of the original crystalline form IV change with temperature. In the ED pattern of form IV at 35 °C, the 040 and the 0 ±2 ±2 reflections are the most intense ones. At 150 °C, the ED pattern of the same zone still shows very well defined reflections at almost the same positions as for T=35 °C but the relative intensities of the reflections are different. At 150 °C, the most intense reflections correspond to the 020 and the 0 ±1 ±1 reflections. As a matter of facts, when cooling down the sample to 30°C, the original pattern of form IV is recovered, which underlines the reversibility of the form IV→ form III transition. This result indicates that form III is "isostructural" to form IV *modulo* the alkyl side chains that are crystallized in form IV and molten in form III. To verify this point, the ED pattern of form III for the [100] zone was calculated from the model of structure of form IV but without alkyl side chains. Figure S1 shows the calculated ED pattern for the structure without alkyl side chains. As observed for T=150 °C, the most intense reflections in the calculated pattern correspond indeed to the 0 ±1 ±1 reflections observed in the experimental ED pattern. This result confirms the strong analogy in the structure of form IV and III.

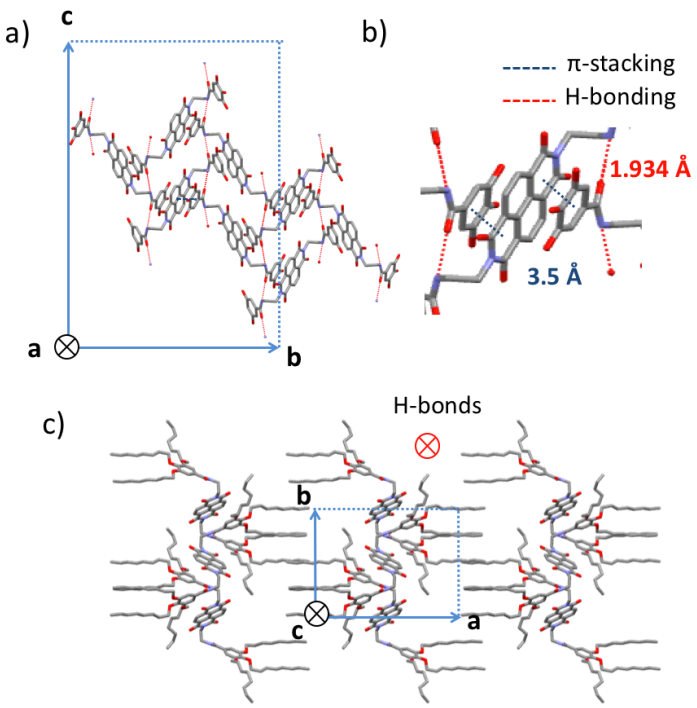


**Figure 9**. Representation along the **a** and **c** axes of the crystal lattice of form III of NDI2. The upper inset is an enlarged view of an NDI core π-stacked between two phenyl units of two adjacent dendrons. Red doted lines show H-bonds between amide groups whereas blue doted lines show short π-stacking distances.

## IV. Discussion.

In various examples from the recent literature on NDI-derivatives, the π-stacking tendency of NDI is strongly affected when it is linked to another π-conjugated unit. The π-stacking depends on the flexibility of the linker between both π-conjugated units. In the absence of a flexible linker i.e. in the case of alkoxyphenyl N-substituted NDIs, long range π-stacking between NDI is observed in a slipped cofacial configuration i.e. with limited π-orbital overlaps.[33] In these compounds, the phenyls that are directly linked to the NDI cannot π-stack. In the case of *N*,*N*′-bis-[(pyridin-4-yl)meth-yl]naphthalene bisimide, π-stacking is observed only between the pyridine units separated from NDI by a flexible $CH_2$ group and thus no π-

stacking is observed between the NDIs.[42] In the polymer p(NDI2OD-T2), NDIs alternate with bithiophene units in the polymer backbone.[43] This alternated copolymer shows two type of stackings present in two polymorphs. In form I, NDI and bithiophene make segregated stacks whereas in form II, a mixed stacking between NDI and bithiophene is observed. Mixed stacks involving NDI and a second conjugated unit are well known when NDI is co-crystallized with some electron–rich groups such as 1,5-dialkoxynaphthalene.[44-46] Well known examples of such assemblies are the so-called aedamer oligomers investigated by Iverson et al. in which the 1,5-dialkoxynaphthalene tethered to the NDI block via a flexible linker folds back onto NDI and stacks with it.[44,45] This short review through existing NDI structures highlights the natural tendency of NDI to π-stack with other conjugated units, especially with electron-rich ones. This is due to the electron-deficient character of the NDI unit. In the present case, phenyl rings and NDI units stack together, possibly because phenyl is electron-rich and NDI is electron-deficient. The originality of NDI2 is that each NDI core is sandwiched between two phenyl groups of adjacent molecules that can further H-bond to the molecule bearing the central NDI via the amide groups. From that point of view, NDI2 differs from the foldamers studied by Iverson et al. in the sense that the phenyl-NDI stacking is intermolecular. [45] This is possible only because the $(CH_2)_2$ linker is flexible enough : it allows the phenyl unit to π-stack with the NDI and the amide groups to be H-bonded along the ***c*** axis. Such an arrangement is indeed not possible for steric reasons in case of a single $CH_2$ linker.

To the best of our knowledge, this is the first evidence of such a peculiar stacking of a NDI core with the phenyls of a solubilizing side group. This result is very interesting as it demonstrates that the lateral trialkoxyphenyl dendrons bearing amide groups that are initially used as scaffolding units can interfere with the conjugated NDI core and impede long-range π-stacking of NDIs. The role of the two lateral dendrons in such systems is not limited to self-assembling and scaffolding via H-bonding between amides, but the phenyls of the dendrons

can π-stack with NDI and therefore hinder the buildup of π-stacked NDI columns. It can be anticipated that the position of the amide group and the length of the flexible alkyl spacer influences strongly the electronic properties of such NDI derivatives.[47,48]

**V. Conclusion.**

The original polymorphism of a H-bonded napthalene bisimide organogelator has been uncovered by a combination of low-dose TEM, AFM, X-ray diffraction, UV-vis and FTIR spectroscopies. Four polymorphs including the dried gel phase, a metastable LC phase, a lamellar and a crystalline form were evidenced. A phase diagram explaining how the structures can be interconverted has been established. Both the polymorphism as well as the structures formed by NDI2 illustrate the subtle interplay between heterocyclic π-stacking of NDI/phenyl and H-bonding between amides. In the metastable LC phase, NDI2 molecules form supramolecular $6_1$ helices made of pairs of H-bonded NDI2 molecules. These $6_1$ helices are further packed in a so-called frustrated trigonal unit cell similar to that observed recently for a perylene bisimide analogue. The observation of such frustrated hexagonal-like structures for two different H-bonded π-gels indicates that helical assemblies are quite common for this class of molecules. In addition, NDI2 forms an original crystal structure (form IV) such that each NDI core is π-stacked between two phenyl cycles of two adjacent NDI2 molecules. This packing impedes long range π-stacking of NDI cores. Overall, these results illustrate the diversity of stacking possibilities for NDI derivatives and the potential wealth of polymorphs accessible for a single organogelator molecule because of the interplay between H-bonding and π-stacking. The exact role of the flexible linker separating the H-bonding unit (amide) from the π-conjugated core (NDI or PBI) needs to be clarified. Preliminary results indicate that no such complex polymorphism is observed for longer $(CH_2)_4$ linkers. A systematic comparison of supramolecular structures as a function of the length of the flexible linker between the

solubilizing dendron and the NDI core is therefore necessary to better understand the processing-structure-property relations for this class of original π-conjugated molecules.

**Acknowledgments.** B. Lotz is acknowledged for fruitful discussions and reading the manuscript. The ANR is acknowledged for financial support. (ANR grant). M. D. acknowledges financial support from Région Alsace.

**Supporting information.**

Synthesis of NDI2. Table listing the solvents inducing gelation, precipitation or solubilization of NDI2. Table giving the transition temperatures and enthalpies between the four polymorphs. TEM ED patterns *versus* temperature showing the transition form III → form IV. FTIR spectra *versus* temperature showing the transition form III → form IV. TEM rotation-tilt diffraction experiment showing the trigonal structure of Form II. Cif file of the structure of NDI2 form IV.

**Conflicts of interest.**

The authors declare no conflicts of interest.

**References**

(1) Hoeben, F. J. M.; Jonkheijm, P.; Meijer, E. W.; Schenning, A. P. H. J. About Supramolecular Assemblies of π-Conjugated Systems. *Chem. Rev.* **2005**, 105, 1491–1546.

(2) Zhan X.; Facchetti A.; Barlow S.; Marks T. J.; Ratner M. A.; Wasielewski M. R.; Marder S. R. Rylene and Related Diimides for Organic Electronics. *Adv. Mater.* **2010**, 23, 268–284.

(3) Würthner, F.; Saha-Möller, C. R.; Fimmel, B.; Ogi, S.; Leowanawat, P.; Schmidt, D. Perylene Bisimide Dye Assemblies as Archetype Functional Supramolecular Materials. *Chem. Rev.* **2016**, 116, 962–1052.

(4) Shukla, D.; Nelson, S. F.; Freeman, D. C.; Rajeswaran, M.; Ahearn, W. G.; Meyer, D. M.; Carey, J. T. *Chem. Mater.* **2008**, 20, 7486–7491.

(5) Chen, Z.; Debije, M. G.; Debaerdemaeker, T.; Osswald, P.; Würthner, F. *ChemPhysChem* **2004**, 5, 137–140.

(6) Jones, B. A.; Facchetti, A.; Wasielewski, M. R.; Marks, T. J. Tuning Orbital Energetics in Arylene Diimide Semiconductors. Materials Design for Ambient Stability of N-Type Charge Transport. *J. Am. Chem. Soc.* **2007**, *129*, 15259–15278.

(7) Oh, J. H.; Liu, S.; Bao, Z.; Schmidt, R.; Würthner, F. Air-Stable N-Channel Organic Thin-Film Transistors with High Field-Effect Mobility Based on N,N′-Bis(heptafluorobutyl)-3,4:9,10-Perylene Diimide. *Appl. Phys. Lett.* **2007**, *91*, 212107.

(8) Basak, S.; Nanda, J.; Banerjee, A. Assembly of Naphthalenediimide Conjugated Peptides: Aggregation Induced Changes in Fluorescence. *Chem. Commun.* **2013**, 49, 6891-6893.

(9) Mukhopadhyay, P.; Iwashita, Y.; Shirakawa, M.; Kawano, S.; Fujita, N.; Shinkai, S. Spontaneous Colorimetric Sensing of the Positional Isomers of Dihydroxynaphthalene in a 1D Organogel Matrix. *Angew. Chem.* **2006**, 118, 1622–1625.

(10) Ghule, N. V.; Bhosale, R. S.; Puyad, A. L.; Bhosale, S. V.; Bhosale, S. V. Naphthalenediimide Amphiphile Based Colorimetric Probe for Recognition of Cu2+ and Fe3+ Ions. *Sens. Actu. B Chem.* **2016**, 227, 17–23.

(11) Jones, B. A.; Facchetti, A.; Marks, T. J.; Wasielewski, M. R. Cyanonaphthalene Diimide Semiconductors for Air-Stable, Flexible, and Optically Transparent N-Channel Field-Effect Transistors. *Chem. Mater.* **2007**, *19*, 2703–2705.

(12) See, K. C.; Landis, C.; Sarjeant, A.; Katz, H. E. Easily Synthesized Naphthalene Tetracarboxylic Diimide Semiconductors with High Electron Mobility in Air. *Chem. Mater.* **2008**, *20*, 3609–3616.

(13) Balakrishnan, K.; Datar, A.; Naddo, T.; Huang, J.; Oitker, R.; Yen, M.; Zhao, J.; Zang, L. Effect of Side-Chain Substituents on Self-Assembly of Perylene Diimide Molecules: Morphology Control. *J. Am. Chem. Soc.* **2006**, *128* (22), 7390–7398.

(14) Delgado, M. C. R.; Kim, E.-G.; Filho, D. A. da S.; Bredas, J.-L. Tuning the Charge-Transport Parameters of Perylene Diimide Single Crystals via End And/Or Core Functionalization: A Density Functional Theory Investigation. *J. Am. Chem. Soc.* **2010**, *132* (10), 3375–3387.

(15) Molla, M. R.; Ghosh, S. Structural Variations on Self-Assembly and Macroscopic Properties of 14,5,8-Naphthalene-Diimide Chromophores. *Chem. Mater.* **2011**, *23*, 95–105.

(16) Marty, R.; Nigon, R.; Leite, D.; Frauenrath, H. Two-Fold Odd–Even Effect in Self-Assembled Nanowires from Oligopeptide-Polymer-Substituted Perylene Bisimides. *J. Am. Chem. Soc.* **2014**, *136*, 3919–3927.

(17) Tsukada, Y.; Nishimura, N.; Mizuguchi, J. It *N*,*N*′-Bis(2-phenyl-ethyl)naphthalene-1,8:4,5-bis(dicarboximide), *Acta Cryst. E* **2008**, *64*, o5.

(18) Mizuguchi, J. Electronic Characterization of N,N′-bis(2-Phenylethyl)perylene-3,4:9, 10-Bis(dicarboximide) and Its Application to Optical Disks. *J. Appl. Phys.* **1998**, *84*, 4479–4486.

(19) Mizuguchi, J.; Hino, K.; Tojo, K. Strikingly Different Electronic Spectra of Structurally Similar Perylene Imide Compounds. *Dyes and Pigments* **2006**, *70*, 126–135.

(20) Klebe, G.; Graser, F.; Hädicke, E.; Berndt, J. Crystallochromy as a Solid-State Effect: Correlation of Molecular Conformation, Crystal Packing and Colour in Perylene-3,4:9,10-Bis(dicarboximide) Pigments. *Acta Crystallographica Section B* **1989**, *45*, 69–77.

(21) Sarbu, A.; Biniek, L.; Guenet, J.-M.; Mesini, P. J.; Brinkmann, M. Reversible J- to H-Aggregate Transformation in Thin Films of a Perylenebisimide Organogelator. *J. Mater. Chem. C* **2015**, *3*, 1235–1242.

(22) Sarbu, A.; Hermet, P.; Maurin, D.; Djurado, D.; Biniek, L.; Diebold, M.; Bantignies, J.-L.; Mesini, P.; Brinkmann, M. Supramolecular Organization of a H-Bonded Perylene Bisimide Organogelator Determined by Transmission Electron Microscopy, Grazing Incidence X-Ray Diffraction and Polarized Infra-Red Spectroscopy. *Phys. Chem. Chem. Phys.* **2017**, *19*, 32514–32525.

(23) Babu, S. S.; Praveen, V. K.; Ajayaghosh, A. Functional π-Gelators and Their Applications. *Chem. Rev.* **2014**, 114, 1973–2129.

(24) Ogi, S.; Stepanenko, V.; Sugiyasu, K.; Takeuchi, M.; Würthner, F. Mechanism of Self-Assembly Process and Seeded Supramolecular

Polymerization of Perylene Bisimide Organogelator. *J. Am. Chem. Soc.* **2015**, *137*, 3300–3307.

(25) Lee, C. C.; Grenier, C.; Meijer, E. W.; Schenning, A. P. H. J. Preparation and Characterization of Helical Self-Assembled Nanofibers. *Chem. Soc. Rev.* **2009**, 38, 671–683.

(26) Marty, R.; Szilluweit, R.; Sánchez-Ferrer, A.; Bolisetty, S.; Adamcik, J.; Mezzenga, R.; Spitzner, E.-C.; Feifer, M.; Steinmann, S. N.; Corminboeuf, C.; et al. Hierarchically Structured Microfibers of "Single Stack" Perylene Bisimide and Quaterthiophene Nanowires. *ACS Nano* **2013**, 7, 8498–8508.

(27) Bu, L.; Pentzer, E.; Bokel, F. A.; Emrick, T.; Hayward, R. C. Growth of Polythiophene/Perylene Tetracarboxydiimide Donor/Acceptor Shish-Kebab Nanostructures by Coupled Crystal Modification. *ACS Nano* **2012**, *6*, 10924–10929.

(28) Brinkmann, M.; Graff, S.; Wittmann, J.-C.; Chaumont, C.; Nuesch, F.; Anver, A.; Schaer, M. and Zuppiroli, L. *J. Phys. Chem. B* **107**, 2003, 10531.

(29) "M86-E01078 APEX2 User Manual", Bruker AXS Inc., Madison, USA, 2006.

(30) Sheldrick, G. M. *Acta Cryst.* **1990**, A46, 467-473.

(31) Sheldrick, G. M. *Acta Cryst.* **2008**, A64, 112-122.

(32) Kohan, M. in Nylon Plastics handbook, Wilmington: Hanser, 1995.

(33) Shukla, D.; Nelson, S. F.; Freeman, D. C.; Rajeswaran, M.; Ahearn, W. G.; Meyer, D. M.; Carey, J. T. Thin-Film Morphology Control in Naphthalene-Diimide-Based Semiconductors: High Mobility N-Type Semiconductor for Organic Thin-Film Transistors. *Chem. Mater.* **2008**, *20*, 7486–749

(34) Bantignies, J.-L.; Vellutini, L.; Sauvajol, J.-L.; Maurin, D.; Wong Chi Man, M.; Dieudonné, P.; Moreau, J. J. E. Hydrogen bonding in self organized lamellar hybrid silica, *J. Non-Cryst. Sol.* **2004**, *345–346*, 605–609.

(35) Snyder, R. G.; Strauss, H. L.; Elliger, C. A.; Carbon-hydrogen stretching modes and the structure of n-alkyl chains. 1. Long, disordered chains *J. Phys. Chem.* **1982**, *86*, 5145–5150.

(36) MacPhail, R. A.; Strauss, H. L.; Snyder, R. G.; Elliger, C. A. ; Carbon-hydrogen stretching modes and the structure of n-alkyl chains. 2. Long, all-trans chains *J. Phys. Chem.* **1984**, *88*, 334–341.

(37) Crick, F. H. C.; Rich, A. The Structure of Collagen. *Nature* **1955**, 176, 780 ;

(38) Cochran, W. ; Crick, F. H. C. and Vand, V. The structure of synthetic polypeptides. I. The transform of atoms on a helix. *Acta Cryst.* **1952**, 5, 581.

(39) Dickerson, R. E.; Geis, I. *The structure and action of proteins*; Harper and Row: New York.

(40) Percec, V.; Peterca, M.; Tadjiev, T.; Zeng, X.; Ungar, G.; Leowanawat, P.; Aqad, E.; Imam, M. R.; Rosen, B. M.; Akbey, U.; et al. Self-Assembly of Dendronized Perylene Bisimides into Complex Helical Columns. *J. Am. Chem. Soc.* **2011**, *133* (31), 12197–12219.

(41) Percec, V.; Sun, H.-J.; Leowanawat, P.; Peterca, M.; Graf, R.; Spiess, H. W.; Zeng, X.; Ungar, G.; Heiney, P. A. Transformation from Kinetically into Thermodynamically Controlled Self-Organization of Complex Helical Columns with 3D Periodicity Assembled from Dendronized Perylene Bisimides. *J. Am. Chem. Soc.* **2013**, *135*, 4129–4148.

(42) M. Nicolas-Gomez, D. Martinez-Otero, A Dorazco-Gonzalez Crystal structure of *N,N'*-bis[(pyridin-4-yl)methyl]naphthalene diimide. *Acta Cryst.* **2014**, E70, 2014, o985- o 986.

(43) Brinkmann, M.; Gonthier, E.; Bogen, S.; Tremel, K.; Ludwigs, S.; Hufnagel, M.; Sommer, M. Segregated versus Mixed Interchain Stacking in Highly Oriented Films of Naphthalene Diimide Bithiophene Copolymers. *ACS Nano* **2012**, *6*, 10319–10326.

(44) Reczek, J. J.; Villazor, K. R.; Lynch, V.; Swager, T. M.; Iverson, B. L. Tunable Columnar Mesophases Utilizing C2 Symmetric Aromatic Donor−Acceptor Complexes. *J. Am. Chem. Soc.* **2006**, *128*, 7995–8002.

(45) Zych, A. J.; Iverson, B. L. Synthesis and Conformational Characterization of Tethered, Self-Complexing 1,5-Dialkoxynaphthalene/1,4,5,8-Naphthalenetetracarboxylic Diimide Systems. *J. Am. Chem. Soc.* **2000**, *122*, 8898–8909.

(46) Martinez, C. R.; Iverson, B. L. Rethinking the Term “pi-Stacking.” *Chem. Sci.* **2012**, *3*, 2191–2201.

(47) Kolhe, N. B.; Devi, R. N.; Senanayak, S. P.; Jancy, B.; Narayan, K. S.; Asha, S. K. Structure Engineering of Naphthalene Diimides for Improved Charge Carrier Mobility: Self-Assembly by Hydrogen Bonding, Good or Bad? *J. Mater. Chem.* **2012**, *22*, 15235.

(48) Kalita, A.; Subbarao, N. V. V.; Iyer, P. K.; Large-Scale Molecular Packing and Morphology-Dependent High Performance Organic Field Effect Transistor by Symmetrical Naphthalene Diimide Appended with Methyl Cyclohexane. *J Phys. Chem. C* **2015**, *119*, 12772-12779